Volume 1 | Number 1 | Jan 2013 | Pages 1–100

Journal of
Materials Chemistry C

Materials for optical and electronic devices
www.rsc.org/materialsC

ROYAL SOCIETY
OF CHEMISTRY

ROYAL SOCIETY
OF CHEMISTRY

www.rsc.org/materialsC

Journal Name

COMMUNICATION

ROYAL SOCIETY OF CHEMISTRY

Supramolecular Polymeric Micelles as High Performance Electrochemical Materials

Chih-Chia Cheng,[a]* Feng-Chih Chang,[b] Fu-Hsiang Ko,[c] Feng-Chun Yu,[b] Yen-Ting Lin,[c] Yeong-Tarng Shieh,[d] Jem-Kun Chen,[e] Duu-Jong Lee[f,g]

A new adenine-functionalized polythiophene (PAT) has been developed which allows an incorporation of self-constituted with multiple hydrogen-bonded groups into micelles. After encapsulation of fullerene derivatives (PCBM) into PAT, their excellent electrochemical storage capacities make the PAT/PCBM micelle a promising candidate for electron storage/transport layer in the fabrication of high-performance electrochemical device.

Conjugated polymer-based resistive switching materials have attracted considerable attention in recent years.[1,2] The unique material characteristics introduce many benefits in aspect of cost effective, flexible structure property, operation of processing, and excellent electrical behaviours (from both localized and delocalized electrons).[3] Polythiophene (PT) is one of the most widely used conjugated polymer, showing good thermal stability and unique optoelectronic characteristics.[4,5] A recent research has been published and extensively investigated the donor-acceptor (D-A) blending system, constructed from PT (PT, an electron donor) and phenyl-C61-butyric acid methyl ester (PCBM, an electron acceptor). The complementary nature of PT/PCBM blending system brings excellent material performance, which is suitable in applying for organic thin-film transistors and photovoltaic cells.[6-8] However, a series of recent reports indicate that PT/PCBM phases tend to segregate over tens of nanometers forming PCBM-rich clusters and crystalline domains of PT.[9-11] The segregation situation eventually results in the bilayer structures.[12] Therefore, there is a challenge to find synthetic methods to improve the nano-morphology of the PT/PCBM blending.

Supramolecular interactions, including hydrogen bonding, metal-ligand coordination and π-π stacking, have been extensively studied in order to understand the mechanisms of self-assembly process in supramolecular chemistry, and also to support constructing new materials with desirable functions and properties.[13] Supramolecular interactions are strongly recognized to influence material properties and in connection with the hydrophilic or hydrophobic chemical properties to form the self-assembly amphiphiles.[14-17] By introducing supramolecular interactions into syntheses of PTs may lead to alteration of amphiphilic feature in the body. Such interactions with further initiate forming physically cross-linked, and stabilize in both aqueous and organic solvents.[18,19] However, supramolecular PTs are still rarely used nowadays. The main reason is because of the hydrophobic backbone and weak intermolecular interactions in the high competitive solvents. Therefore intention of controlling supramolecular assembly and amphiphilic structure with conjugated polymers remains a challenging and interesting topic to be studied.

A series synthetic methods of nucleobase-functionalized conjugated polymers were developed, which exhibits excellent photoelectronic properties and thermal stability.[20-23] The nucleobase complex played a very important role in the light emission process. Due to the formation of stable physically cross-linked structure, it is fabricated into phosphorescent organic light-emitting devices (OLED) with excellent performance and high ability of hole-transporting.[21,23] These studies revealed many features of forming nanostructures, transferred from binding and recognition properties in optoelectronic research field into non-covalent systems. Based on the above discussion, we assumed that introducing nucleobase into PT/PCBM system with an effective energy transferring may affect their nanostructures and further packing on arrangement behavior significantly. Meanwhile we provide a potential application in electronics and energy storage devices. In this study, a new π-conjugated PT containing pendant adenine groups (PAT) has been successfully synthesized by using a three-step process. PAT is able to initiate self-assemble process into

a. Graduate Institute of Applied Science and Technology, National Taiwan University of Science and Technology, Taipei 10607, Taiwan.
E-mail: cccheng@mail.ntust.edu.tw
b. Institute of Applied Chemistry, National Chiao Tung University, Hsinchu 30050, Taiwan.
c. Department of Materials Science and Engineering, National Chiao Tung University, Hsinchu 30050, Taiwan.
d. Department of Chemical and Materials Engineering, National University of Kaohsiung, Kaohsiung 81148, Taiwan.
e. Department of Materials Science and Engineering, National Taiwan University of Science and Technology, Taipei 10607, Taiwan.
f. Department of Chemical Engineering, National Taiwan University of Science and Technology, Taipei 10607, Taiwan.
g. Department of Chemical Engineering, National Taiwan University, Taipei 10617, Taiwan.
Electronic Supplementary Information (ESI) available:. See DOI: 10.1039/x0xx00000x

Journal of Materials Chemistry C Accepted Manuscript

physically cross-linked structure through the intermolecular adenine-adenine (A-A) interaction. It can be easily fabricated into micelles in dimethyl sulfoxide (DMSO) solution. In theory, not only micelles can be manipulated into groups according size and shape, but micellar organization can also be used as a functionally cargo nano-container for quintessential nanomaterials. In order to prove this argument, we observed the incorporation of hydrophobic PCBM will affect the encapsulation process of PAT micelle and cause a substantial increase in micelle size. The fabrication of PAT/PCBM micelle shows unique photophysical properties and the electrochemical storage capacity. The results support a reliable reproducibility and stability of PAT/PCBM micelle in the solid state, which is a promising candidate for non-volatile memory devices. When the PAT/PCBM micelle is applied as an electron storage/transport layer (ESTL) in a multilayer memory device, it exhibited versatile memory characteristics, including a tunable threshold voltages (from 5.5 to 16.4 V), high ON/OFF current ratio ($>10^4$), and stable resistive switching behavior. Thus, PAT/PCBM micelle can be tailored to improve storage performance, which is expected to construct of high-stable and energy-efficient device.
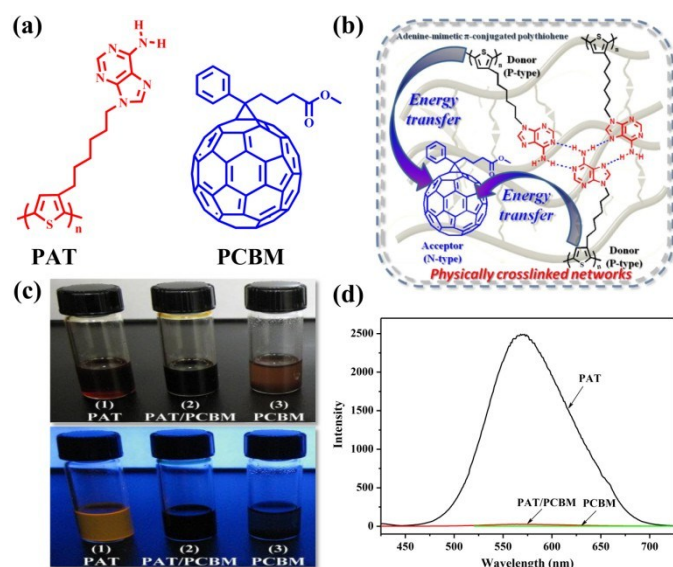

Fig. 1 Self-assembly of conjugated polymer into supramolecular micelles and encapsulation of PCBM nanoparticles. (a) Chemical structures of PAT and PCBM. **(b)** Graphical representation of energy within supramolecular self-assembled networks. **(c)** Comparison of solubility characteristics by the digital photographs between PAT, PAT/PCBM and PCBM in DMSO, simultaneously exposed under natural light (upper panel) and UV lamp illumination (lower panel). **(d)** PL emission spectra of PAT, PAT/PCBM and PCBM in DMSO solution.

Synthesis and phsical properties of a new adenine-functionalized polythiophene (PAT). A heterocyclic adenine-functionalized thiophene monomer, 6-amino-9-[6-(thiophen-3-yl)hexyl]purine, synthesized using the illustrated mechanism as described in Supporting Information and Scheme S1. The isolated monomer was subsequently subjected to oxidative polymerization in the presence of $FeCl_3$, aiming at producing a low-regioregular PT containing pendant adenine groups. The structural formula of the

formed PAT is shown in Fig. 1a, which was recovered in high yield (63%), with the resulting PAT exhibiting an acceptable regioregularity 56%. It is in category of low polydispersity index (PDI = 1.24) with ca. 10 repeat units, determined by measured results from NMR, GPC and MALDI-TOF MS (Figs. S2-S4). In order to investigate the dynamic behavior of PAT in the strong non-covalent self-interactions, both dynamic scanning techniques Fourier transform infrared (FTIR) and differential scanning calorimetry (DSC) measurements were performed, results are shown in Figs S5 and S6, respectively. Fig. S5 illustrates the N-H and C=N stretching region of the FT-IR spectra of PAT. The spikes appeared at 3120 and 3297 cm^{-1} is corresponding to the stretching vibration of the hydrogen-bonded N-H groups, and the characteristic peak at 1679 cm^{-1} is from the contribution of hydrogen-bonded C=N.[24-26] In addition, it shows that the A-A interactions between PAT chains were not destroyed during the heating process from 30 to 150 °C. It was demonstrated that the PAT formed a tight network of hydrogen-bonded interactions in the bulk state. Fig. S6 shows the DSC thermogram for adenine-functionalized monmer which exhibits a discrete melting temperature (T_m) at 174 °C. Furthermore, we observe a slightly change in the thermal curve, which represents the glass transition temperature of PAT (T_g = 138 °C) and it gives an evidence of the formation of low regioregular structure. This implies that the hydrogen bonding motif in the bulk plays a specific and significant role in controlling the miscibility between the adenine groups and PT chains,[20,22] which further results in the formation of homogeneous materials with continuous physical properties.[13] Therefore PAT is recommend as an advanced derivate for the multiple use of comprehensive applications, such as advanced optoelectronic devices.

Conjugated polymer-based supramolecular micelles to effectively encapsulate PCBM. Adenine molecule, with self-complementary hydrogen bonds, shows a property of self-assemble into a network structure.[27,28] By driving energy transferred from the donor fluorophore to the acceptor molecule (D-A interaction), PAT can generate a stable complex with PCBM. It demonstrates a considerable control over material morphology, which helps the formation of well-ordered nanostructures using bottom-up assembly process of PAT/PCBM mixture (Fig. 1b). This phenomenon attracted our dramatic interests in understanding the dynamic and hydrogen bonding behavior of PAT/PCBM in a solution. In terms of the solubility tests, PAT is only dissolved in polar DMSO, whereas hydrophobic PCBM is completely undissolved in DMSO (Fig. 1c and Fig. S7). The presence of adenine groups in PAT enables the formation of intermolecular hydrogen-bond networks. Surprisingly, a PAT/PCBM mixture is able to be dissolved in DMSO and forms solution in dull-red color. When the solution was projected using UV light with 365 nm wavelength, the emission light is totally quenched due to the formation of a stable complex between PAT and PCBM (Fig. 1c). In order to investigate this phenomenon, we compared the photoluminescence (PL) properties of PAT solution, with/without existence of PCBM (Fig. 1d). The measurements of PL are consistent with the photographic results: all samples were dissolved in DMSO, PL emission spectra showed the maximum peak at 572 nm in the PAT solution; oppositely this peak was absent in the PAT/PCBM (1:1 weight ratio) or pure PCBM solution system. We

COMMUNICATION

supposed this phenomenon is due to the energy was transferred to the absorbed photon, further resulting in the fluorescence quenches. According to the observations mentioned above, it is suggested that the formations of micelles and highly stable complexes in DMSO due to the hydrogen bond network between adenine units of PAT and the PAT/PCBM mixture. These intriguing results lead our interests to further investigate on the self-assembly system in solution state.
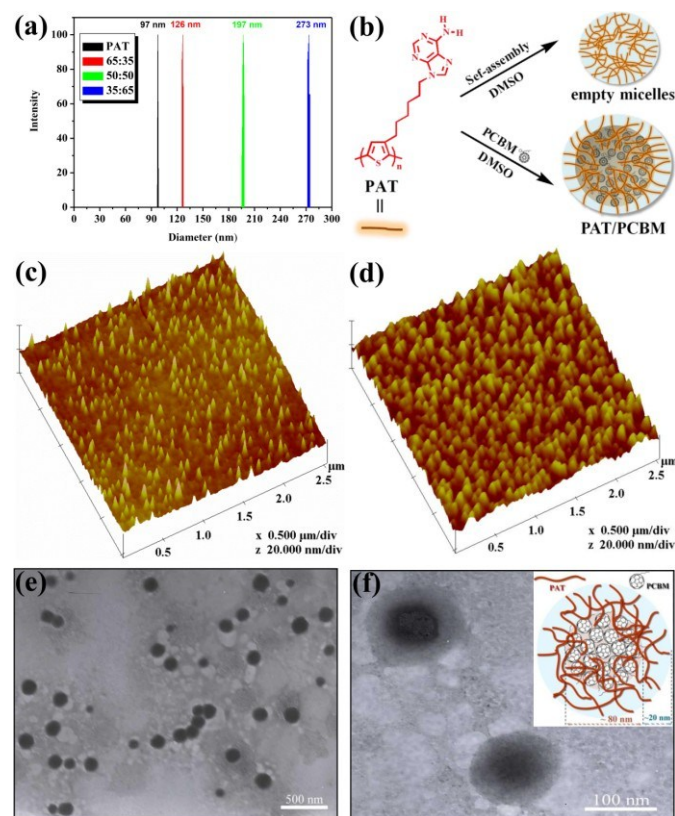

Fig. 2 High efficient encapsulation of hydrophobic PCBM in PAT nanoparticles by simple solvent-blending method. (a) DLS analyses of PAT micelles with different amounts of PCBM. (b) Suggested processes of the formation of empty micelles and core/shell nanoparticles in DMSO solution. AFM images showing the spherical morphology of (c) PAT and (d) 65/35 PAT/PCBM. (e,f) TEM images presenting the core-shell structures of 65/35 PAT/PCBM, as pointed by a cartoon picture in (d), to display the thickness of a core.

In order to understand the structure and encapsulation mechanisms of both systems, we additionally carried out demonstration by measurements of dynamic light scattering (DLS) in DMSO solution at 25 °C. In Fig. 2a, the PAT exhibits one peak at 97 nm with narrow distribution (PDI = 0.01 ± 0.01), implying that large aggregates are formed through A-A hydrogen bonding. Intermolecular bonding is the consequence of physical cross-linking and self-assembly process for the self-locking mechanism, which is also the main cause rather than the anisotropic structures to result in the stability of homogenized micelle (Fig. 2b).[29] Further a great amount of PCBM-encapsulated PAT micelles were prepared using a solvent blending and followed a filtration method (details are presented in Supplementary Information). Surprisingly, such

PAT/PCBM mixtures were purely homogeneous solutions and displayed a narrow mono-modal distribution (PDI = 0.02-0.08 ± 0.02). The particle size of PAT/PCBM micelle was increased gradually from 126 nm to 273 nm with PCBM content increased. As the sample size increased, it was suggested that a micellar expansion was required to accommodate the PCBM molecules in the particle core in order to achieve a high loading content (Fig. 2b). The resulting PCBM-loading efficiency had reached to the maximum value of 33.6%, allowing us to accurately control and adjust loading contents (Table S1). This result indicates that by incorporating PCBM into PAT micelle, an additional D-A interaction was introduced, and it improves loading efficiency of PCBMs significantly. In addition, atomic force microscopy (AFM) and transmission electron microscopy (TEM) analyses were performed to further examine the core/shell structure of the 65/35 PAT/PCBM micelle (Figs. 2c-f and Fig. S8). These images suggested that the spherical structure of the complex was ca. 120 nm in width. Similar results were also observed from the DLS data to show well-constructed core/shell nanostructures. The high-magnification TEM provides clear images (Fig. 2f) for the diameter of the inner core (dark black circles) at around 80 nm, and the light shell thickness at around 20 nm, corresponding to those of the PCBM-rich domain and the PAT-rich domain, respectively. This result supports our hypothesis that the D-A interactions enhance transition of the PCBM groups into the core of the micelles, and thus creates a high loading capacity with narrow size distribution.
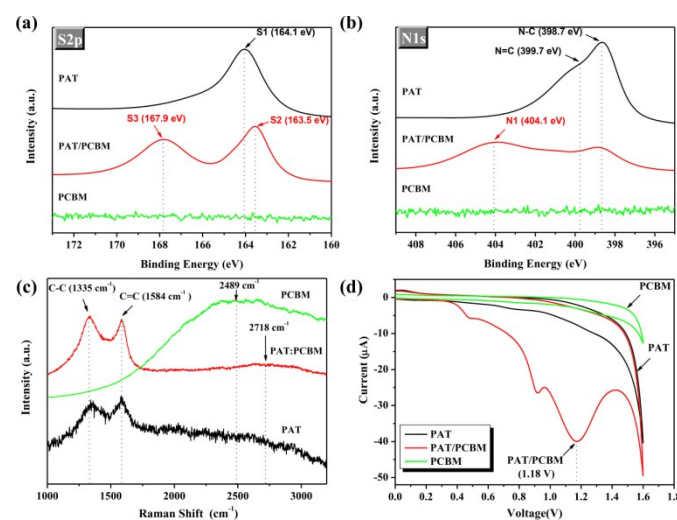

Fig. 3 Characterizations and electrochemical properties of core/shell structured PAT/PCBM nanoparticles. (a) S2p XPS, (b) N1s XPS, (c) Raman spectra and (d) CV traces of PAT, PCBM, 65/35 PAT/PCBM hybrid samples.

Structural recognition and electrochemical properties of PAT/PCBM in bulk state. The core/shell nanostructure, produced using the PAT and PCBM complex, was analysed using x-ray photoelectron spectroscopy (XPS) experiments, which helped with characterising the structural relationship of the PAT/PCBM complex. In Fig. 3a, results of S2p XPS contributed by PAT, PCBM and 65/35 PAT/PCBM nanoparticle are presented. It shows that three dominant peaks at 163.5, 164.1 and 167.9 eV were observed, corresponding to sulfur atoms in different binding environments.

The presence of a broad peak at 164.1eV (S1) indicates that the sulfur atoms of pure PAT are doublet structures, due to the spin-orbit coupling of the $S2p_{3/2}$ and $S2p_{1/2}$ energy levels.[30,31] For the PAT/PCBM complex results, the peak at 164.1 eV (S1), which is originally shown in PAT curve, slightly shifted to the lower binding energy $S2p_{3/2}$ band at 163.5 eV (S2).[31] In addition, a new peak at 167.9 ev (S3) appears to reflect a specific binding of PCBM bound in connection with the sulfur atom,[32] meaning that a change in the nature of the PAT/PCBM interface. Similar results are also observed from N1s spectra, shown in Fig. 3b. An additional peak at 404.1 ev (N1) belonging to the PAT/PCBM complex is presented, suggesting the evidence of intermolecular energy transferring between conjugated PCBM and the nitro N1s sites of adenine.[33] Although A-A interactions are formed in the shell segment, the complex formation of PAT/PCBM was noticeable in the solid state. Because the presence of a physically cross-linked network is difficult to move or rotate in solid state, and thus improves the structural stability of core–shell nanoparticles and a significant increase in energy transfer. The electron affinity of PCBM is in favour of PAT. Therefore we assume that the energy transfer mechanism within PAT/PCBM complex structure is the most important factor in relation with the formation of a stable core/shell nanoparticle, as illustrated in Figs. 1b and 2b.

Further investigation on the energy transfer behavior was carried out using Raman spectroscopy measurements, demonstrated in Fig. 3c. It shows that two peaks at 1335 and 1584 cm^{-1}, contributed from the PAT, are believed to be the consequences of C–C and C=C stretching vibrations of low-regioregular polymer backbones.[34] The measurements of PCBM present a broad spectrum containing a photoluminescence signal (2489 cm^{-1}) with overlapping Raman bands.[35] As expected, the results of PAT/PCBM complex shows evidence that the intensity of the C-C band is stronger than the C=C band due to the energy transfer between PAT and PCBM.[34] It is interesting to notice that the photoluminescence intensity of PAT/PCBM nanoparticle is substantially dropped off and moving towards to a higher wavenumber (2718 cm^{-1}) due to transfer characteristics (compared to the PCBM results). The spectrum implies that the activity of incorporating PCBMs into the core of supramolecular micelles strongly influences their excitonic properties of the luminescence. On the other hand, it also provides a possibility to "trap" energy by confining electron motion in core/shell nanostructures, meaning that the stored energy can be accumulated quickly in the core layer. This electrochemical storage character was further investigated via cyclic voltammetry (CV) measurement. We used ferrocene as an internal standard and tetrabutylammonium hexafluorophosphate as an electrolyte. The measuring results are summarized in Fig. 3d. It is particularly noteworthy that the reduction peak of current at 1.18 V was significantly enhanced from -2.8 μA to -41.2 μA for the PAT/PCBM nanoparticle, which showed a good current carrying capability compared to the pure PAT and PCBM. The increases current signal shows capability relative to confining the spreading electrons in the PCBM core. The observations also suggest that the presence of the core/shell structure and intra-core clusters is of crucial importance for electric storage. It can strongly modulate the electrical properties of the conjugated PCBM through D-A energy transfer. As a result, the electrochemical and capacitive characteristics of

PAT/PCBM nanoparticles support a potential application in the fabrication of electrochemical memory devices.
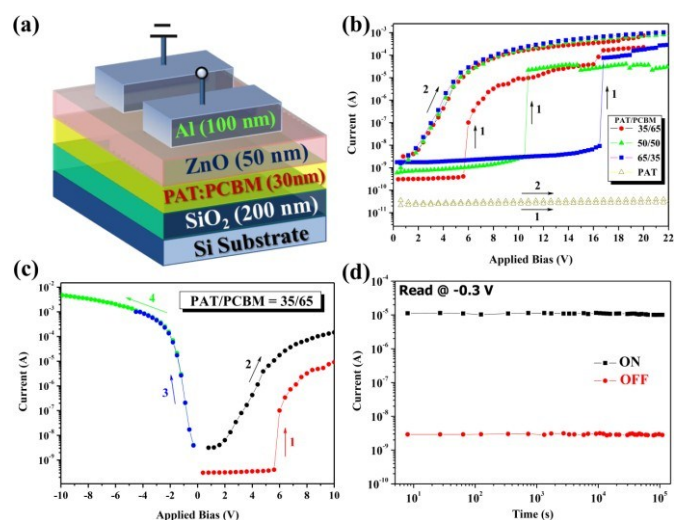

Fig. 4 Supramolecular core/shell nanoparticles exhibiting electro-induced memory effect. (a) Structural configuration of multilayer memory device. **(b,c)** Current-voltage (I-V)characteristics of PAT/PCBM-based devices. **d)** Data retention of 35/65 PAT/PCBM device.

Nonvolatile memory devices using supramolecular core/shell PAT/PCBM electrets. In order to evaluate the memory performance, a three layered organic memory device consisted of the following structural configuration was prepared: wafer/silicon dioxide (SiO_2, 200 nm)/ESTL (PAT/PCBM, 30 nm)/Zinc oxide (ZnO, 50 nm)/Aluminum (Al, 100 nm), illustrated in Fig. 4a. The electrical curve of tested current varies with voltage of the devices is collected and shown in Fig. 4b. It is observed that only a low current with the external applied voltage condition are presented for the neat PAT-based device, due to its natural insulating properties. When various amounts of the PCBM were added into the PAT, each PAT/PCBM nanoparticle exhibits a significant electrical transition during the voltage sweeps and switches (from the OFF state to ON state). It also shows the threshold voltage of 65/35 PAT/PCABM complex (16.6 V) is much higher than that of 50/50 complex (10.5 V). Further increases the PCBM content to 65 wt%, the threshold voltage decreases to 5.6 V, indicating an inverse trend for threshold voltage with PCBM content. This phenomenon is partly due to the enhancement of localized charge carriers into a polaronic state.[36] In the presence of high content of PCBM, charge carriers tend to increase the charging speed and storage-capacity of the intra-cluster medium. Electrical scanning at the device, based on the 35/65 (PAT/PCBM) nanoparticle composition, is further investigated with four boundary conditions: 0 to 10 V (for sweep 1 to 2), 0 to -4.0 V (sweep 3), and 0 to -10 V (sweep 4). The results are shown in Fig. 4c. After the first positive sweep for charging storage, this device cannot return to its initial state (OFF state) nor applies a reverse-bias voltage. In other words, this electronic transition in the first sweep can function as a ''writing'' process for the memory device. The current is maintained in a "conducting" state for the subsequent positive sweep from 0 to 10 V (sweep 2) and positive sweep from 0 to 10 V (sweeps 3-4). This phenomenon suggests that

the non-volatile memory characteristics of the SiO$_2$/(PAT/PCBM)/ZnO structure with an ON/OFF current ratio is up 10^6 at -2.0 V. In addition, it is noteworthy that the positive and negative bias voltages can affect the device performance significantly at the low voltage zone (Fig. S9). The current value at -2 V is ca. 5 order of magnitude higher than the result at +2 V. We assume that this is highly possibility that an electric polarization effect on discharge features of spherical core/shell nanostructures.[37] The device of 35/65 nanoparticle was applied a negative bias voltage (-0.3 V), and the retention time measurement for both ON and OFF states was collected periodically. As shown in Fig. 4d, the ON/OFF current ratio exceeded 10^4 without any degradation of the electric performance. The results have further shown that the physically cross-linked PTC-A shell is suggested as a direct pathway for electron transport/confinement, which has improved memory performance significantly. In addition, the enhanced performance is also attributed to improved charge carrier balance in the PCBM core and obtaining excellent retention properties, due to the effective energy transfer between PAT and PCBM. Therefore, our current research are fully dedicated on further improving the lifetime of non-volatile caches and enhancing the charge-transportation efficiency by optimizing the performance characteristics of fast storage devices.

Conclusions

In summary, a new adenine-functionalized polythiophene (PAT) has been developed and characterized. PAT is able to proceeding self-assemble process in the crosslinked structure through the intermolecular A-A interaction, which can be easily fabricated into micelles in DMSO solution. The produced micelle is in size of a small diameter about 97 nm with a narrow distribution (PDI = 0.01), which helps create its highly stable structure and being able to carry out a high efficiency loading process. We also observed that the incorporation of hydrophbic PCBM into PAT affected the micellization process of PAT micelles, and thus enabled the fine-tuning of PCBM loading capability. When the PAT/PCBM micelle is applied as an ESTL in a trilayer memory device, the constructed device exhibits non-volatile switching behavior with a tunable threshold voltage (from 5.6 to 16.6 V), excellent ON/OFF current ratio (>10^4), and long retention time (>10^5 s). PAT/PCBM is the first example of supramolecular micelle possessing high electron affinity properties, providing a potential route towards next-generation data storage/memory materials.

Acknowledgements

Notes and references

1.   F. J. M. Hoeben, P. Jonkheijm, E. W. Meijer and A. P. H. J. Schenning, *Chem. Rev.*, 2005, **105**, 1491.
2.   Q. D. Ling, D. J. Liaw, C. Zhu, D. S. H. Chan, E. T. Kang and K. G. Neoh, *Prog. Polym. Sci.*, 2008, **33**, 917.
3.   (a) Q. D. Ling, E. T. Kang, K. G. N, Y. Chen, X. D. Zhuang, C. Zhu and D. S. H. Chan, *Appl. Phys. Lett.*, 2008, **92**,143302. (b) N. H. You, C. C. Chueh, C. L. Liu, M. Ueda and W. C. Chen, *Macromolecules*, 2009, **42**, 4456. (c) T. Kuorosawa, C. C. Chueh, C. L. Liu, T. Higashihara, M. Ueda and W. C. Chen, *Macromolecules*, 2010, **43**, 1236. (d) X. D. Zhuang, Y. Chen, G. Liu, B. Zhang, K. G. Neoh, E. T. Kang, C. X. Zhu, Y. X. Li and L. J. Niu, *Adv. Funct. Mater.*, 2010, **20**, 2916. (e) Y. K. Fang, C. L. Liu, C. Li, C. J. Lin, R. Mezzenga and W. C. Chen, *Adv. Funct. Mater.*, 2010, **20**, 3012. (f) X. D. Zhuang, Y. Chen, B. X. Li, D. G. Ma, B. Zhang and Y. Li, *Chem. Mater.*, 2010, **22**, 4455. (g) X. D. Zhuang, Y. Chen, G. Liu, P. P. Li, C. X. Zhu, E. T. Kang, K. G. Neoh, B. Zhang, J. H. Zhu and Y. X. Li, *Adv. Mater.*, 2010, **22**, 1731. (h) C. L. Liu and W. C. Chen, *Polym. Chem.*, 2011, **2**, 2169. (i) G. Liu, B. Zhang, Y. Chen, C. X. Zhu, L. Zeng, D. S. H. Chan, K. G. Neoh, J. Chen and E. T. Kang, *J. Mater. Chem.*, 2011, **21**, 6027. (j) Y. K. Fang, C. L. Liu and W. C. Chen, *J. Mater. Chem.*, 2011, **21**, 4778. (k) Y. Chen, B. Zhang, G. Liu, X. Zhuang and E. T. Kang, *Chem. Soc. Rev.*, 2012, **41**, 4688. (l) B. Zhang, G. Liu, Y. Chen, C. Wang, K. G. Neoh, T. Bai and E. T. Kang, *ChemPlusChem*, 2012, **77**, 74. (m) W. Zhang, C. Wang, G. Liu, J. Wang, Y. Chen and R. W. Li, *Chem. Commun.*, 2014, **50**, 11496.
4.   S. Wang, Y. P. Qu, S. J. Li, F. Ye, Z. B. Chen and X. N. Yang, *Adv. Funct. Mater.*, 2014, **25**, 748.
5.   B. Tsang, C. Q. Yu and S. Granick, *ACS Nano.*, 2014, **8**, 11030.
6.   E. J. Meijer, D. M. de Leeuw, S. Setayesh, E. van Veenendaal, B. H. Huisman, P. W. M. Blom, J. C. Hummelen, U. Scherf and T. M. Klapwijk, *Nature Materials*, 2003, **2**, 678.
7.   Y. Kim, S. Cook, S. M.Tuladhar, S. A. Choulis, J. Nelson, J. R. Durrant, D. D. C. Bradley, M. Giles, I. McCulloch, C. S. Ha and M. Ree, *Nature Materials*, 2006, **5**, 197.
8.   G. Li, R. Zhu and Y. Yang, *Nature Photonics*, 2012, **6**, 153.
9.   T. Savenije, J. E. Kroeze, X. Yang and J. Loos, *Adv, Funct. Mater.*, 2005, **15**, 1260.
10. G. Dennler, M. C. Scharber and C. J. Brabec, *Adv. Mater.*, 2009, **21**, 1323.
11. I. A. Howard, R. Mauer, M. Meister and F. Laquai, *J. Am. Chem. Soc.*, 2010, **132**, 14866.
12. C. W. Rochester, S. C. Mauger and A. J. Moulé, *J. Phys. Chem. C.*, 2012, **116**, 7287.
13. T. Aida, E. W. Meijer and S. I. Stupp, *Science*, 2012, **335**, 813.
14. T. F. A. Greef and E. W. Meijer, *Nature*, 2008, **453**, 171.
15. G. Chen and M. Jiang, *Chem Soc Rev*, 2011, **40**, 2254.
16. E. Busseron, Y. Ruff, E. Moulin and N. Giuseppone, *Nanoscale*, 2013, **5**, 7098.
17. P. Wei, X. Yan and F. Huang, *Chem. Soc. Rev.*, 2015, **44**, 815.
18. X. Zhang and C. Wang, *Chem. Soc. Rev.*, 2011, **40**, 94.
19. S. Seiffert and J. Sprakelc, *Chem. Soc. Rev.*, 2012, **41**, 909.
20. C. C. Cheng, Y. L. Chu, P. H. Huang, Y. C. Yen, C. W. Chu, A. C. M. Yang, F. H. Kuo, J. K. Chen and F. C. Chang, *J. Mater. Chem.*, 2012, **22**, 18127.
21. Y. L. Chu, C. C. Cheng, Y. C. Yen and F. C. Chang, *Adv. Mater.*, 2012, **24**, 1894.
22. C. C. Cheng, Y. S. Wang, F. C. Chang, D. J. Lee, L. C. Yang and J. K. Chen, Chem. Commun., 2015, **51**, 672.
23. C. C. Cheng, Y. L. Chu, F. C. Chang, D. J. Lee, Y. C. Yen, J. K. Chen, C. W. Chu and Z. Xin, *Nano Energy*, 2015, **13**, 1.
24. Y. Kyogoku, R. C. Lord and A. Rich, *J. Am. Chem. Soc.*, 1967, **89**, 496.
25. F. Ilhan, M. Gray and V.M. Rotello, *Macromolecule*, 2001, **34**, 2597.
26. C. C. Cheng, C. F. Huang, Y. C. Yen and F. C. Chang, *J. Polym. Sci., Part A: Polym. Chem.*, 2008, **46**, 6416.
27. M. Furukawa, H. Tanaka and T. Kawai, *Surface Science*, 2000, **445**, 1.
28. R. E. A. Kelly, W. Xu, M. Lukas, R. Otero, M. Mura, Y.J. Lee, E. Lægsgaard, I. Stensgaard, L.N. Kantorovich and F. Besenbacher, *Small*, 2008, **4**, 1494.
29. K. M. Zero and R. Pecora, *Macromolecules,* 1982, **15**, 87.

30. S. Yang, L. Zhi, K. Tang, X. Feng, J. Maier and K. Müllen, *Adv. Funct. Mater.*, 2012, **22,** 3634.

31. F. Buckel, F. Effenberger, C. Yan, A. Gölzhäuser and M. Grunze, *Adv. Mater.*, 2000, **12**, 901.

32. T. Antoun, R. Brayner, F. Fiévet, M. Chehimi and A. Yassar, *Eur. J. Inorg. Chem.*, 2007, 1275.

33. F. D'Souza, S. Gadde, D. M. Islam, S. C. Pang, A. L. Schumacher, M. E. Zandler, R. Horie, Y. Araki and O. Ito, *Chem. Commun.*, 2007, 480.

34. A. Chunder, J. H. Liu and L. Zhai, *Macromol. Rapid Commun.*, 2010, **31**, 380.

35. E. Klimov, W. Li, X. Yang, G. Hoffmann and J. Loos, *Macromolecules*, 2006, **39**, 4493.

36. E. Lioudakis, I. Alexandrou and A. Othonos, *Nanoscale Res. Lett*. 2009, **4**, 1475.

37. A. Ibrala, A. Zouitine, E. M. Assaid, H. E. Achouby, E. M. Feddi and F. Dujardin, *Physica B: Condensed Matter* 2015, **458**, 73.

Graphical Abstract
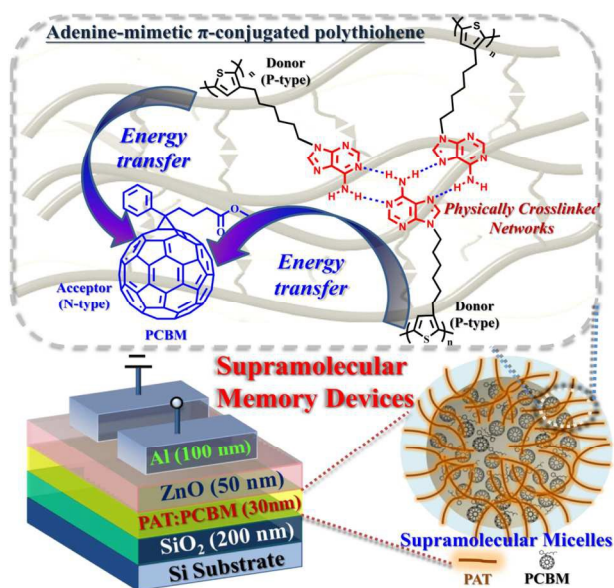
Core-shell supramolecular micelles exhibit excellent memory performances, providing a potential route towards next-generation energy storage/memory materials.